machines

MDPI

Article

Unified Design Methodology for a Polycentric Transfemoral Knee Prosthesis Using Kinematic Synthesis †

Mertcan Koçak * and Erkin Gezgin

Department of Mechatronics Engineering, İzmir Katip Çelebi University, 35620 Izmir, Turkey; erkin.gezgin@ikcu.edu.tr

* Correspondence: mertcan.kocak@ikcu.edu.tr

† This paper is an extended version of our published paper Koçak, M.; Gezgin, E. Utilization of Kinematic Synthesis Methodology on a Novel Polycentric Mechanism for Transfemoral Knee Prosthesis. In Proceedings of the Mechanism Design for Robotics (MEDER 2024), Timişiora, Romania, 27–29 June 2024.

Abstract: This study introduces a novel single-degree-of-freedom polycentric knee mechanism specifically designed for transfemoral prostheses to address dual challenges of stability during the stance phase and biomimetic motion during the swing phase. Leveraging analytical kinematic synthesis, the proposed mechanism integrates separate kinematic designs for each of the gait phases into a combined structure that prevents singularity issues during full knee flexion, which is a significant limitation in conventional active designs. The stance phase mechanism emphasizes stability through precise control of the instantaneous center of rotation (ICR) and weight-bearing support, while the swing phase mechanism adopts a biomimetic motion trajectory. In order to validate the proposed methodology, kinematic synthesis, numerical simulations, and visual analyses were conducted. Incorporating insights from polycentric prostheses and orthotic applications, the proposed mechanism achieves a seamless transition between two different configurations by keeping its overall mobility. Additionally, its possible compatibility with motorized actuation offers a foundation for active prosthesis systems, paving the way for adapting the advantages of polycentric prosthesis to active devices. This innovative approach offers a scientifically grounded pathway for improving transfemoral prosthetic systems, advancing both their biomechanical utility and user comfort.

Keywords: transfemoral prostheses; kinematic synthesis; structural synthesis; polycentric mechanism

check for updates

Academic Editors: Marco Ceccarelli and Erwin Lovasz

Received: 1 December 2024
Revised: 23 December 2024
Accepted: 28 December 2024
Published: 31 December 2024

Citation: Koçak, M.; Gezgin, E. Unified Design Methodology for a Polycentric Transfemoral Knee Prosthesis Using Kinematic Synthesis. *Machines* **2025**, *13*, 20. https://doi.org/10.3390/machines13010020

Copyright: © 2024 by the authors. Licensee MDPI, Basel, Switzerland. This article is an open access article distributed under the terms and conditions of the Creative Commons Attribution (CC BY) license (https://creativecommons.org/licenses/by/4.0/).

1. Introduction

Amputation, a critical surgical intervention, entails the removal of a limb or a portion of it due to various causes, including trauma, chronic disease, severe infections, and surgeries to remove bone and muscle tumors [1,2]. While accidents and military conflicts remain significant factors contributing to the incidence of amputations [3,4], in high-income countries, the majority of the cases are attributed to complications arising from vascular diseases and diabetes-related ischemia (a reduction in local blood flow), which, together, constitute the primary causes of limb loss [5–7]. As amputation rates continue to rise, particularly for lower extremities, demand for prosthetic solutions personalized to individual needs increases. Projections suggest that the global population of individuals with lower limb amputations could be doubled by 2050 [6], underscoring an urgent need for advancements in prosthetic technology to enhance both the functionality and accessibility of these devices. Such progress holds the potential to not only improve the quality of life for amputees, but also address the required healthcare demands of the growing population.

The main objectives in the development of transfemoral (above-knee) prostheses center on enhancing user stability and safety while assisting a smooth reintegration into daily activities [8]. Achieving these objectives requires the continual advancement in both the mechanical design and control systems of prosthetic devices, alongside an in-depth analysis of the human walking gait cycle to better replicate natural walking [9]. Despite the significant research and development in transfemoral prostheses driven by recent technological advancements, fully replicating the complex biomechanics and sensory feedback of a healthy limb remains a challenging problem that needs an efficient solution [10]. Nevertheless, ongoing studies indicate that closer approximations to natural kinematics are attainable and recent innovations provide encouraging pathways for improvement [11].

The design and development of transfemoral prostheses present unique challenges, as these devices must account for the complex dynamics and stability requirements of the knee joint, which are critical for safe and natural movement. One approach that has shown promising merits in enhancing the naturalness of movement for transfemoral amputees can be given as the implementation of polycentric knee joint mechanisms. Polycentric knee prostheses feature an instantaneous center of rotation (ICR) that shifts during knee flexion and extension in the human's sagittal plane, enabling a movement pattern that provides stable locomotion with safety, by moving the ICR in the proximal direction on the sagittal plane, which promotes a more secure, naturally locking knee position. This proximally located ICR configuration, typically realized through four-bar mechanisms, meets the stability requirements necessary for supporting the user's weight in the stance phase [12,13] and allows a broader range of knee flexion, which translates to increased comfort and functionality, especially in postures requiring significant knee bending, such as sitting [14–18]. Additionally, the combined rotation and sliding movements within these mechanisms facilitate the slight shortening of the limb during locomotion, mimicking the natural knee physiology. This shortening effect reduces the risk of tripping or falling, particularly on uneven or rough terrain, thereby enhancing safety for the user [1,12,15,19–21]. Optimizing these biomechanical attributes, polycentric knee mechanisms continue to push the boundaries of prosthetic design. Given the absence of a universally defined ideal ICR trajectory, prosthetic designs are personalized to align with the physiological capacities of the individual, with the resulting designs categorized based on specific user requirements [12]. However, solely analyzing the ICR trajectory is insufficient to draw comprehensive conclusions regarding the overall functionality of the system [12]. Radcliffe and Deg [13] proposed the flexion stability ratio in order to determine the effect of the ICR trajectory objectively on the stance stability and to create the opportunity for comparing the stability performance of the mechanisms. In this way, it has been shown that dissimilar ICR trajectories can also produce similar stability effects.

A comprehensive review of the literature reveals that the kinematic synthesis of polycentric transfemoral knee mechanisms, primarily four- or six-bar configurations, has largely relied on optimization techniques and computational tools to address design complexities. These optimization methods have been developed to meet a range of user-specific design criteria, which vary according to individual physiological conditions, including body weight, residual limb length, and activity level, thereby personalizing the prosthetic function to individual needs [12,13]. Significant contributions to the optimization of polycentric knee mechanisms include those by Soriano et al. [1], who introduced a new four-bar knee mechanism with optimizing defined design parameters with generic algorithm. Morales-Cruz et al. [22] focused on refining a six-bar mechanism through optimization techniques. Their work provided a viable alternative to graphical and analytical approaches, demonstrating the fact that optimized six-bar configurations could be suitably adapted for knee prosthesis applications. Sancisi et al. [23] contributed to the field similarly by developing

an optimization framework for four-bar mechanisms, emphasizing stability and cosmetic appeal, which are two critical factors in prosthetic design. Another influential study by Marisami and Venkatachalam [24] expanded upon these approaches by optimizing the geometry of polycentric mechanisms based on five key parameters that impact stability and oscillatory motion. This study, utilizing a computational model, produced a prototype that validated the leg shortening and ICR alignment with the established stability criteria. In a recent work by Wang et al. [25], a novel polycentric hybrid knee prosthesis was presented containing an active actuation with simply converting a four-bar mechanism to a six-bar mechanism, when desired. The authors validated stair ascent in the active mode and the mode transition through specified subject tests in the work, including two mechanism syntheses, four-bar linkage for the passive mode and six-bar linkage for the active mode, together with carrying out the mode transition in between. In work [26], a simple kinematic model was presented, synthesizing a four-bar knee prosthesis by considering Radcliffe's flexion stability ratio and comparing the performance of the simulations in terms of stability and toe clearance. Further studies in the field have consistently explored the effectiveness of polycentric systems through diverse optimization algorithms and computational methodologies, rather than relying solely on analytical methods [27–30].

Collectively, these studies underscore the adaptability and effectiveness of polycentric designs in transfemoral prostheses. Leveraging computational optimizations, the recent research continues to refine the precision and efficiency of these mechanisms, advancing the capacity to approximate natural gait dynamics. However, there remains an ongoing need for further innovation in both of the optimization techniques and prosthetic designs to address the complex biomechanical demands of amputees, particularly in terms of stability on uneven surfaces and adaptability to diverse physical activities [31–35], and a polycentric mechanism design to achieve different tasks such as providing coordination between knee and ankle joint movements with a six-bar linkage structure to allow transfemoral amputees to sit in the squatting posture [36] or to improve mediolateral balance for amputees during walking [37].

Unlike the stance phase that requires an increased ICR on the sagittal plane for achieving stability, as the gait cycle transitions to the swing phase, the ICR ideally needs to move closer to the anatomical center of the knee in the distal direction, facilitating a smoother and more comfortable rotation. Radcliffe [35] indicates the position change manner of the ICR during a gait cycle, providing improved voluntary control of knee stability. This shift, although beneficial for natural movement, often necessitates passing through a singularity point in four-bar designs, which presents a significant limitation for active prosthetic mechanisms. The inherent singularity that occurs during this transition phase imposes constraints on the prostheses' range of motion and stability, particularly in dynamic and uneven terrains. Due to this challenge, active or semi-active control mechanisms are frequently avoided in transfemoral prosthetics to decrease the instability caused by the singularity effect, which leads to the rareness of works on active polycentric knee prostheses [38–40].

In light of these challenges, the current study addresses the mentioned critical issue by focusing on strategies to minimize or entirely avoid singularities throughout the gait cycle, with the goal of maintaining a stable ICR trajectory that supports both the stance and swing phases without compromising the prosthetic structural integrity. Drawing insights from mechanisms traditionally used in orthoses and exoskeletons, which also aim to replicate the physiological joint motion without encountering singularities, it aimed to enhance the usability and comfort of polycentric prosthetic knees for transfemoral amputees. By doing so, it aimed to fill the gap between stability and flexibility requirements, thus enhancing the functional capabilities of prosthetic knee mechanisms.

Throughout the design processes for orthoses and exoskeletons, the precise replication of the natural knee ICR trajectory becomes a main critical design goal instead of reaching stability during the stance phase, as there exists no limb loss in the application area. Since these devices are intended to assist rather than replace joint function, their kinematic alignments with natural movement patterns of the knee are vital. Consequently, studies in this field often aim to closely match the knee's natural ICR trajectory, which reflects the anatomical complexities of human knee motion [16]. During locomotion, the knee can move dependently in three different human axes, flexion/extension on the sagittal plane, abduction/adduction on the frontal plane, and internal/external rotation on the transverse plane, among which the majority of the movement occurs perpendicular to the sagittal plane compared to the other mentioned planes in minor amounts, which are generally ignored during designing processes. Accordingly, by using the fact that cruciate ligaments act as inextensible fibers connecting the femur and tibia, the knee joint's anatomy only on the sagittal plane is represented effectively as a crossed four-bar linkage [41], where the model simplifies the anatomical structure, allowing for comparisons between the knee prosthesis motion and natural kinematics generated by the given mechanism [42].

This complexity has led to a variety of methodological approaches within the literature to measure the natural knee centroid trajectory [43]. Among these, one of the most widely adopted methods involves the utilization of X-ray genograms to capture the ICR path during motion [44]. Notably, the study proposed by Walker et al. [45] has gained prominence for its comprehensive extraction of knee trajectory data based on cadaver and volunteer studies. These provided an approximate average trajectory that serves as a reliable model for design applications, although individual variations in ICR trajectory occur due to unique anatomical differences. Walker's work remains a foundational reference in the field, offering a standard trajectory model widely applied in orthotic designs. Subsequent research has frequently adopted Walker's trajectory model as a basis for developing polycentric orthoses and exoskeletons, illustrating its robustness and utility in diverse applications [46,47]. Olinski et al. [46] synthesized a four-bar linkage mechanism designed to follow the ICR trajectory as projected onto the sagittal plane by utilizing Walker's trajectory model. The authors' approach involved optimization based on functional criteria, allowing them to refine the mechanism's performance in simulation, particularly in terms of achieving smoother, anatomically aligned movement. Similarly, Bertomeu et al. [47] optimized an anti-parallel four-bar mechanism to align with the ICR trajectory established by Walker's model. Their work focused on refining the flexion and extension behavior of the mechanism to match the natural movement path, which enhances the design's applicability for knee orthotic and exoskeleton devices.

In light of the given literature, the current study seeks to further refine polycentric knee mechanisms by integrating insights from the approaches in literature to enhance prosthetic functionality and user comfort. This body of work underlines the importance of precise kinematic modeling in assistive devices and provides valuable insights for the further development of polycentric prosthetic mechanisms. Given these considerations, the primary objective of the paper is to develop a single-degree-of-freedom (DoF) polycentric mechanism while avoiding singularities during knee flexion. To achieve this, a unique analytical kinematic design approach is proposed to allow the opportunity for active actuator integration, enabling a prosthetic system capable of adaptive stability and biomimetic motion across varying gait phases to simulate natural knee function better. This modular approach allows for the personalized adaptation of the mechanism based on individual user characteristics, such as activity level, weight, and anatomical differences, thus aiming to address the diverse and dynamic needs of transfemoral amputees. The introduced

modular framework combines separate designs for the stance and swing phases within a unified adaptable structure.

By employing analytical kinematic synthesis methods, the proposed design framework enables a user-specific flexion angle modification, effectively optimizing prosthetic performance across gait phases. This modularization along with the presented design allows for an overall mobility configuration that remains consistent, while altering the designed structure between the stance to swing phase kinematics by the user's individual needs. Through this approach, it aimed to establish a scientifically grounded, analytically driven foundation for creating transfemoral prosthetic systems that present a new framework to the literature to be applied, ultimately enhancing functionality and comfort for end users.

This paper is organized as follows: Section 2 presents the structural design and constraints. Individual kinematic synthesis methodologies for both the stance and swing phases are carried out in Section 3. The conceptual design with an engineering approach and resultant numerical example are introduced in Section 4. The work's limitations, discussions, and future direction are given in Section 5. In Section 6, the work is concluded. This paper presents an extended version of the paper "Utilization of Kinematic Synthesis Methodology on a Novel Polycentric Mechanism for Transfemoral Knee Prosthesis", which was presented at the MEDER 2024 6th Symposium on Mechanism Design for Robotics, held in Timisoara (Romania) on 27–29 June 2024 [48].

2. Structural Design and Constraints

Enhancing the authors' previous work [48], the design procedure of single-DoF polycentric transfemoral knee prosthesis is proposed in order to establish a novel methodology that minimizes the reliance on optimization techniques by employing an analytical approach. Utilizing the proposed methodology, any personalized prosthetic design can be realized more effectively by adapting design constraints that specifically provide individual user requirements. The proposed framework integrates two distinct mechanisms that operate in harmony with a single-DoF input, thereby fulfilling the unique demands of both the stance and swing phases within the gait cycle in a single innovative kinematic topology. This integration requires a single input to mimic knee joint motion through a shared component of the system.

At the outset of the structural design and constraints definition, distinct requirements for the stance and swing phases must be addressed. While the primary focus in this study is on advancing prosthetic design, an examination of orthotic design principles is also required due to the novelty that we tried to introduce. Traditional four-bar polycentric mechanisms can achieve an angular range of approximately 120 degrees during full flexion. On the other hand, singularities along their motion limit their applicability in active polycentric designs. Therefore, for the stance phase, the ICR of the polycentric mechanism is strategically positioned within the stability zone to enhance knee joint stability, depending on the desired stability level of the individual based on the activity level, weight, etc. Here, it is important to note that, as Radcliffe and Deg [13] mentioned, the instant location and trajectory of the ICR during the stance phase can be diverse within various prosthetics; yet, their performance can be compared by the flexion stability ratio. Conversely, for the swing phase, the ICR is expected to move in the distal direction on the sagittal plane towards the natural ICR region of the knee, facilitating comfortable and natural flexion as given in [35].

Figure 1a is dedicated to showing the approximate positioning of the traditional four-bar mechanism and its ICR trajectory on the sagittal plane. The coupler link of the mechanism is rigidly connected to the pylon tube to replicate the tibia with the functionality of the shank. The location of the coupler's ICR trajectory stems from the proximal side of the femur to give a natural stability and tends to move in the distal direction on the sagittal

plane with increasing knee flexion to meet requirements. The traditional parallel four-bar mechanism with structural details is illustrated in Figure 1b, which will be utilized in the stance phase design. If this mechanism is employed during full flexion, as observed in most passive polycentric transfemoral prostheses, it will inevitably encounter a singularity point. The adaptability of four-bar mechanisms in kinematic synthesis allows for infinite design variations [35], making an analytical approach advantageous in developing personalized solutions for diverse user-specific design criteria.

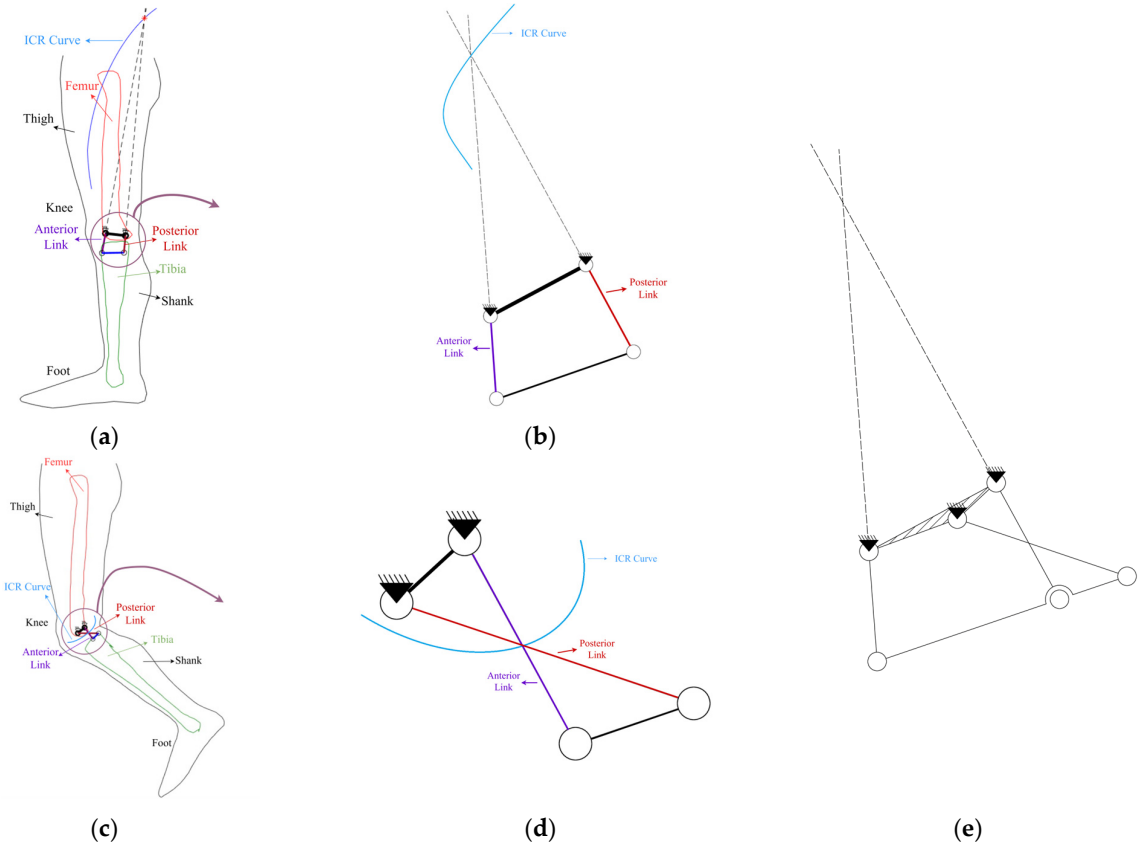


Figure 1. Structural design flow [48]: (**a**) stance phase mechanism on knee; (**b**) stance phase kinematic structure; (**c**) swing phase mechanism on knee; (**d**) swing phase kinematic structure; and (**e**) coarsely combined mechanism kinematic structure around stance–swing transition moment.

In the swing phase, the ICR must approximate the natural knee level to support more biomimetic, anatomically aligned movement, similar to those in orthotic applications. By using an anti-parallel four-bar mechanism, which would look like the structure formed by the anterior and posterior cruciate ligaments, it is possible to guide the ICR to align with the natural knee rotation center, promoting both comfort and functionality. This kind of structure can be positioned approximately around the knee joint as illustrated in Figure 1c. This design approach, commonly seen in orthotic applications, reduces the risk of singularities and improves rotational movement by imitating ligament function. Additionally, to accommodate activities requiring high flexion, such as sitting, the ICR must descend rapidly to the knee's natural level to maintain ergonomic movement and aesthetic alignment [18]. The structural details of the given anti-parallel four-bar mechanism, illustrated in Figure 1d, are utilized in the swing phase design. However, if this configuration is employed during full flexion, stability issues may arise in the stance phase due to its inherent tendency to bend easily.

The integration of these phase-specific requirements into a single, unified structure introduces a significant novelty: a combined kinematic framework that can achieve a single-

DoF knee flexion within the sagittal plane. This integration is realized through the use of a shared link, where the posterior link of the stance mechanism simultaneously serves as the anterior link of the swing mechanism, as illustrated in Figure 1e. During the stance phase, the ICR specific to this phase must be utilized, while, in the swing phase, the ICR defined for that phase governs the mechanism's motion. To enable a seamless transition between these phases, it is critical to define the positioning of the combined mechanism at the stance-to-swing transition point by imposing appropriate design constraints. This requires an engineering solution to adapt the structure of the combined mechanism while preserving its mobility. However, a structural analysis of the combined mechanism reveals a zero-mobility configuration, which creates an inherent mobility limitation, demanding an additional DoF. The solution to this mobility issue is discussed in the following section.

3. Kinematic Synthesis

The repetitive movements of the gait cycle in the sagittal plane, where the majority of human locomotion occurs, necessitate a deeper analysis to define the required motion. From the perspective of the transfemoral prosthesis design, the exact motion associated with this cycle can be described by three DoFs, which are subdivided into two primary components: the two-DoF planar ICR trajectory and the single-DoF flexion angle required at corresponding specific instances in repetitive motion. Thus, designing a mechanism to perfectly replicate this exact motion without error would require a three-DoF system. However, from a mechanism design perspective, such an approach would likely result in over-engineering. To address this, a key objective in polycentric mechanism design is to achieve the required motion with a single-DoF. This simplifies the mechanical complexity while maintaining functionality within an acceptable margin of error. The approach aligns with the principles of kinematic synthesis, which involves determining the geometry and dimensions of a mechanism to fulfill a specific task or motion efficiently [49,50]. By adopting this methodology, the proposed design aims to balance mechanical simplicity with the practical requirements of human locomotion: basically, the kinematic synthesis forms of three customary tasks for kinematic synthesis as function generation, path generation, and body-guidance or motion generation. The specific kinematic synthesis methodology for planar mechanisms, detailed in prior works [51–54], is particularly suited for this type of application, allowing for a structured reduction in DoF while retaining an effective motion characteristic. In the subsequent sections, two distinct kinematic synthesis application processes are represented for the stance and swing phases, integrating the required structural design parameters and constraints previously discussed to achieve the intended functional outcomes.

3.1. Kinematic Synthesis for Stance Phase

In this section, while the primary focus is on the design of the stance phase mechanism, where a traditional four-bar mechanism is typically sufficient to meet the functional requirements, the mobility limitation of the combined mechanism must also be addressed. As illustrated in Figure 1e, the initial combined mechanism design exhibits zero mobility if left in its current form. To impart mobility to this mechanism, it is necessary to introduce an additional joint, thereby increasing its DoF.

When employing a traditional four-bar mechanism as the stance phase component, it becomes apparent that the mechanism must satisfy a three-DoF task, despite its inherent single-DoF capacity. Through the application of the kinematic synthesis methodology, discussed in the subsequent paragraphs, it is evident that an additional DoF is required in order to achieve the desired functionality. To resolve this, one of the links is modified to

include a prismatic joint, as shown in Figure 2. Consequently, the mechanism transitions to a two-DoF five-bar configuration with an RRRPR structure.

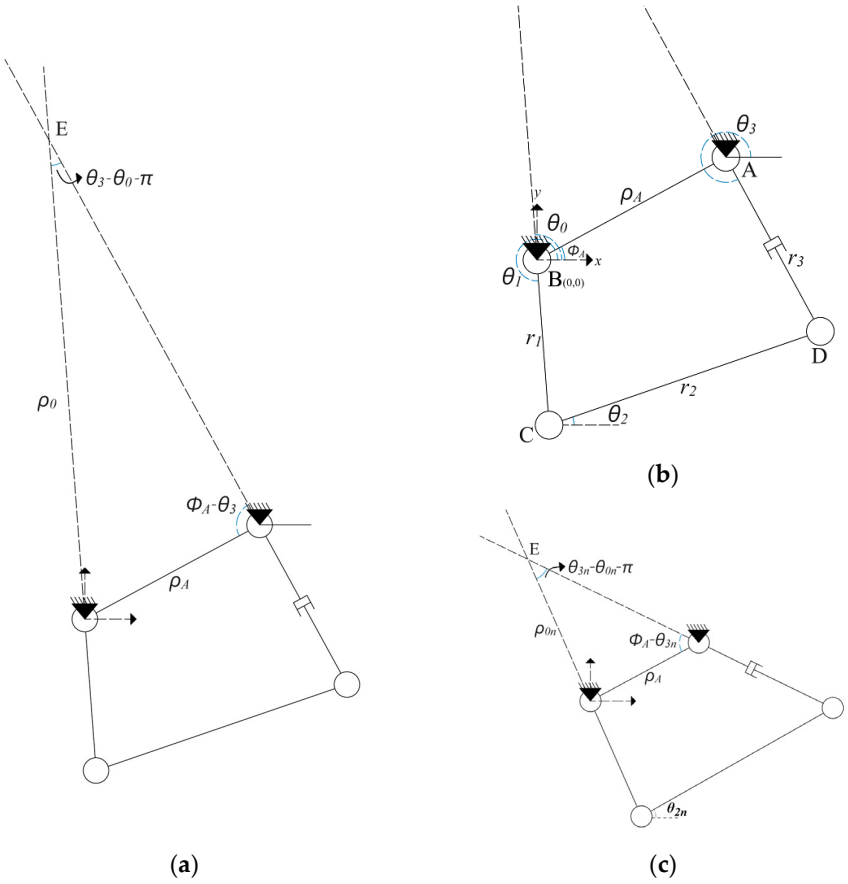


Figure 2. Stance phase kinematic representations [48]: (**a**) Upper triangle parameters; (**b**) stance kinematic structure with parameters; and (**c**) stance–swing phase transition moment parameters.

This approach also effectively addresses the mobility limitation of the combined mechanism by introducing the necessary additional DoFs. The inclusion of the prismatic joint is not only a practical solution but also a natural outcome of the applied kinematic synthesis methodology, ensuring that the mechanism fulfills the required motion while maintaining design feasibility. Nevertheless, focusing exclusively on the stance phase mechanism introduces the issue of transforming it into a two-DoF system, a concern that will be revisited in the context of the swing phase design.

In the mechanism illustrated with its parameters in Figure 2b, the fixed-point B was designated as the origin, while point A, defined by the parameters ρ_A and ϕ_A, was identified as the second grounded point of the initially defined four-bar mechanism (the prismatic joint on the link AD is ignored at start). Both ground points are positioned on the residual limb of the thigh. The pylon tube, which serves as the connection to the foot, is attached to the coupler r_2, the link between the joints on C and D, at a variable flexion angle. During knee flexion, the motion of joints on C and D is governed by the parameters r_1, r_3, θ_1, and θ_3. In this configuration, the angle θ_2 denotes the variation in flexion angle, while point E represents the ICR of the mechanism, which is determined by the parameters ρ_0, θ_0, and θ_3. In the kinematic synthesis process, the trajectory to be followed by point E, along with the corresponding flexion angle θ_2 required to align with this trajectory, are established as key design criteria. The procedure incorporates geometric relationship constraints, as illustrated in Figure 2a, along with the constraints at the stance–swing transition instant

depicted in Figure 2c. This methodology can thus be characterized as a body guidance with a different approach.

Closed loop equations for x and y coordinates and angle relations are given in Equations (1)–(3). From now on, sines and cosines will be shown in a shortcut form, as s and c, respectively.

$$r_1 c\theta_1 + r_2 c\theta_2 = \rho_A c_A + r_3 c\theta_3 \tag{1}$$

$$r_1 s\theta_1 + r_2 s\theta_2 = \rho_A s_A + r_3 s\theta_3 \tag{2}$$

$$\theta_1 = \theta_0 + \pi => s\theta_1 = -s\theta_0 \;\&\; c\theta_1 = -c\theta_0 \tag{3}$$

From the given equations, the following sine and cosine relations can be extracted as in Equations (4) and (5):

$$c\theta_3 = \frac{-r_1 c\theta_0 + r_2 c\theta_2 - \rho_A c_A}{r_3} \tag{4}$$

$$s\theta_3 = \frac{-r_1 s\theta_0 + r_2 s\theta_2 - \rho_A s_A}{r_3} \tag{5}$$

To ensure the tracking of point E in the mechanism depicted in Figure 2a, a geometric constraint is defined using the triangle ABE at the top of the mechanism. Additionally, another crucial constraint involves the transition pose between the stance and swing phases, illustrated in Figure 2c. At this transitional instant, the direction of ED at the end of the stance phase must be determined based on the desired position of the swing phase relative to ICR. It is essential that we ensure that the position of the knee center at the beginning of the swing phase aligns with the direction of ED. In this context, n corresponds to the final precision point within the stance phase. Consequently, the parameters ρ_{0n}, ρ_{3n}, θ_{0n}, and θ_{3n} must be defined for this critical transition instant. In Table 1, the parameters and variables are summarized to be used in the stance phase design, where the r_{3i} is revealed to be the variable after the synthesis procedure is utilized.

Table 1. Stance phase design parameters classification.

Classification	Parameters
Construction Parameters	ϕ_A, r_1, r_2, ρ_A
Known Parameters	Point B (X_B, Y_B), ρ_{0n}, θ_{0n}, ρ_{3n}, θ_{3n}
Known Variables	ρ_{0i}, θ_{0i}, θ_{2i}
Unknown Variable	θ_{3i}, r_{3i}

Considering the geometric constraints, Equations (6) and (7) are obtained by applying the sine theorem:

$$\frac{s(\theta_3 - \theta_0 - \pi)}{\rho_A} = \frac{s(\varnothing_A - \theta_3)}{\rho_0} => \rho_A = \frac{-\rho_0 s(\theta_3 - \theta_0)}{s(\varnothing_A - \theta_3)} \tag{6}$$

$$\frac{-s(\theta_{3n} - \theta_{0n})}{\rho_A} = \frac{s(\varnothing_A - \theta_{3n})}{\rho_{0n}} => \rho_A = \frac{-\rho_{0n} s(\theta_{3n} - \theta_{0n})}{s(\varnothing_A - \theta_{3n})} \tag{7}$$

Given the Equations (6) and (7) are equivalent (ρ_A = ρ_A), this relationship leads to the derivation of Equation (8) and, subsequently, Equation (9):

$$\frac{-\rho_0 s(\theta_3 - \theta_0)}{s(\varnothing_A - \theta_3)} = \frac{-\rho_{0n} s(\theta_{3n} - \theta_{0n})}{s(\varnothing_A - \theta_{3n})} \tag{8}$$

$$(\rho_0 s\theta_3 c\theta_0 - \rho_0 s\theta_0 c\theta_3) s(\varnothing_A - \theta_{3n}) - (\rho_{0n} s\varnothing_A c\theta_3 - \rho_{0n} s\theta_3 c\varnothing_A) s(\theta_{3n} - \theta_{0n}) = 0 \tag{9}$$

When the variables of Equations (4) and (5) are placed into Equation (9), Equation (10) is obtained:

$$\begin{aligned}&\left[\rho_0 c\theta_0\left(\tfrac{-r_1 s\theta_0+r_2 s\theta_2-\rho_A s\varnothing_A}{r_3}\right)-\rho_0 s\theta_0\left(\tfrac{-r_1 c\theta_0+r_2 c\theta_2-\rho_A c\varnothing_A}{r_3}\right)\right][s(\varnothing_A-\theta_{3n})]\\&-\left[\rho_{0n} s\varnothing_A\left(\tfrac{-r_1 c\theta_0+r_2 c\theta_2-\rho_A c\varnothing_A}{r_3}\right)-\rho_{0n} c\varnothing_A\left(\tfrac{-r_1 s\theta_0+r_2 s\theta_2-\rho_A s\varnothing_A}{r_3}\right)\right][s(\theta_{3n}-\theta_{0n})]=0\end{aligned} \tag{10}$$

Upon applying the methodology, it is observed that the r_3 parameter is effectively eliminated, transforming into a variable that changes across different instances. This outcome is a natural consequence of the kinematic synthesis methodology.

By combining the known and unknown parameters, Equation (11) is derived:

$$\begin{aligned}&\left(\tfrac{r_2 s_A}{r_3}\right)[\rho_0 c\theta_{3n} s(\theta_2-\theta_0)-\rho_{0n} c\theta_2 s(\theta_{3n}-\theta_{0n})]+\left(\tfrac{r_2 c_A}{r_3}\right)[-\rho_0 s\theta_{3n} s(\theta_2-\theta_0)+\rho_{0n} s\theta_2\, s(\theta_{3n}-\theta_{0n})]+\left(\tfrac{s_A}{r_3}\right)[\rho_0\rho_{0n} c\theta_0 s(\theta_{3n}-\\&\theta_{0n})]+\left(\tfrac{-c_A}{r_3}\right)[\rho_0\rho_{0n} s\theta_0 s(\theta_{3n}-\theta_{0n})]+\left(\tfrac{r_1 s_A}{r_3}\right)[\rho_{0n} c\theta_0 s(\theta_{3n}-\theta_{0n})]+\left(\tfrac{-r_1 c_A}{r_3}\right)[\rho_{0n} s\theta_0 s(\theta_{3n}-\theta_{0n})]=0\end{aligned} \tag{11}$$

To ease the process, the known and unknown parameters are expressed in polynomial form to define the objective function, arranged as shown in Equation (12):

$$\begin{aligned}&\underbrace{(-r_1)}_{P_0}\underbrace{[\rho_{0n} s\theta_0 s(\theta_{3n}-\theta_{0n})]}_{f_0}+\underbrace{(r_2)}_{P_1}\underbrace{[-\rho_0 s\theta_{3n} s(\theta_2-\theta_0)+\rho_{0n} s\theta_2 s(\theta_{3n}-\theta_{0n})]}_{f_1}+\underbrace{(\tan_A)}_{P_2}\underbrace{[\rho_0\rho_{0n} c\theta_0 s(\theta_{3n}-\theta_{0n})]}_{f_2}\\&+\underbrace{(r_1\tan_A)}_{P_3}\underbrace{[\rho_{0n} c\theta_0 s(\theta_{3n}-\theta_{0n})]}_{f_3}+\underbrace{(r_2\tan_A)}_{P_4}\underbrace{[\rho_0 c\theta_{3n} s(\theta_2-\theta_0)-\rho_{0n} c\theta_2 s(\theta_{3n}-\theta_{0n})]}_{f_4}-\underbrace{[\rho_0\rho_{0n} s\theta_0 s(\theta_{3n}-\theta_{0n})]}_{F}=0\end{aligned} \tag{12}$$

The relevant polynomial is shown in Equation (13):

$$P_0 f_0 + P_1 f_1 + P_2 f_2 + P_3 f_3 + P_4 f_4 - F = 0 \tag{13}$$

Examining the objective function presented in Equation (12) reveals non-linear relationships, as expressed in Equations (14) and (15):

$$P_3 = -P_0 P_2 = \lambda_1 \tag{14}$$

$$P_4 = P_1 P_2 = \lambda_2 \tag{15}$$

Given two non-linear parameter coefficients identified, polynomial expressions are formulated as shown in Equation (16). In order to solve the set of equations, three different construction parameters are required, which are the r_1, r_2, and ϕ_A parameters included in P_0, P_1, and P_2:

$$P_i = l_i + m_i\lambda_1 + n_i\lambda_2 \quad i = 0, 1, 2 \tag{16}$$

By expressing Equation (16) in matrix form for the three structural parameters, the resulting linear and non-linear terms are formulated as shown in Equations (17)–(19):

$$\underbrace{\begin{bmatrix} f_0^1 & f_1^1 & f_2^1 \\ f_0^2 & f_1^2 & f_2^2 \\ f_0^3 & f_1^3 & f_2^3 \end{bmatrix}}_{A}\begin{bmatrix} l_0 \\ l_1 \\ l_2 \end{bmatrix} = \begin{bmatrix} F_1 \\ F_2 \\ F_3 \end{bmatrix} \tag{17}$$

$$[A]\begin{bmatrix} m_0 \\ m_1 \\ m_2 \end{bmatrix} = \begin{bmatrix} -f_3^1 \\ -f_3^2 \\ -f_3^3 \end{bmatrix} \tag{18}$$

$$[A]\begin{bmatrix} n_0 \\ n_1 \\ n_2 \end{bmatrix} = \begin{bmatrix} -f_4^1 \\ -f_4^2 \\ -f_4^3 \end{bmatrix} \tag{19}$$

As a result of specifying the precision points for design purposes, the linear l_0, l_1, and l_2, and non-linear m_0, m_1, m_2, n_0, n_1, and n_2 parameters are determined. By simultaneously solving Equations (20) and (21), derived from the combination of Equations (14)–(16), it becomes possible to compute λ_1 and λ_2:

$$\lambda_1 = -(l_0 + m_0\lambda_1 + n_0\lambda_2)(l_2 + m_2\lambda_1 + n_2\lambda_2) \tag{20}$$

$$\lambda_2 = (l_1 + m_1\lambda_1 + n_1\lambda_2)(l_2 + m_2\lambda_1 + n_2\lambda_2) \tag{21}$$

The polynomial parameters required to obtain the structural parameters can be determined for each λ_1 and λ_2 by using Equation (22):

$$\begin{aligned} P_0 &= l_0 + m_0\lambda_1 + n_0\lambda_2 \\ P_1 &= l_1 + m_1\lambda_1 + n_1\lambda_2 \\ P_2 &= l_2 + m_2\lambda_1 + n_2\lambda_2 \end{aligned} \tag{22}$$

The synthesis is terminated for these three parameters with the relationships shown in Equation (23) between the polynomial coefficients and structural parameters:

$$\begin{aligned} r_1 &= -P_0 \\ r_2 &= P_1 \\ \text{ø}_A &= \text{atan}(P_2) \end{aligned} \tag{23}$$

In light of the presence of all the data in Equation (24), the value of ρ_A can be reached:

$$\rho_A = \frac{-\rho_{0n}\text{s}(\theta_{3n} - \theta_{0n})}{\text{s}(\text{ø}_A - \theta_{3n})} \tag{24}$$

As a result, different θ_3 and r_3 values for each precision point can be found using Equations (25) and (26):

$$\theta_{3i} = atan2(-r_1\text{s}\theta_{0i} + r_2\text{s}\theta_{2i} - \rho_A\text{s}\text{ø}_A, -r_1\text{c}\theta_{0i} + r_2\text{c}\theta_{2i} - \rho_A\text{c}\text{ø}_A) \tag{25}$$

$$r_{3i} = \frac{-r_1\text{s}\theta_{0i} + r_2\text{s}\theta_{2i} - \rho_A\text{s}\text{ø}_A}{\text{s}\theta_{3i}} \tag{26}$$

It is concluded that the mechanism functions as a two-DoF system, as the link r_3 effectively behaves as a prismatic joint based on the derived mathematical expressions.

3.2. Kinematic Synthesis for Swing Phase

For the swing phase, utilizing the mechanism structure illustrated in Figure 1d, efforts were directed towards reducing the mobility of the stance phase mechanism while maintaining the proper orientation of the shared component at transition. The kinematic structure necessary for the swing phase has been designed to mimic the anatomical behavior of the anterior and posterior cruciate ligaments, ensuring a single-DoF movement capability. The parameters for this configuration are illustrated in Figure 3. In addition to the fixed ground point A, the second ground point F is defined using parameters ρ_F and ϕ_F. The stance phase mechanism shares a common dyad, r_3, which includes a prismatic joint to accommodate linear motion.

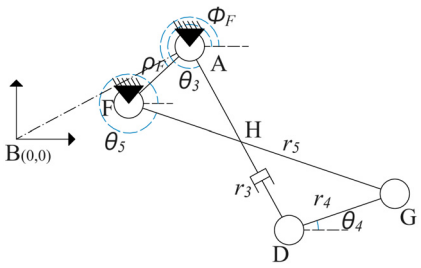


Figure 3. Swing kinematic structure with parameters [48].

In this structure, the coupler r_4, connecting the joints D and G, is linked to the end of r_2, working in coordination to produce the flexion movement necessary for the attached pylon tube. Additionally, link r_5, incorporating a passive rotation angle θ_5, is placed between the grounded point F and joint G. By applying the kinematic synthesis procedures, the dimensions of this configuration can be determined by minimizing the positional error while achieving the overall motion requirement.

The stance phase mechanism initially exhibits two DoFs; however, a critical objective is to reduce the overall DoF to one, aligning with the primary design aim. Similarly, the proposed swing mechanism ensures a reduction to a single-DoF, thereby maintaining consistency in both orientation and the ICR positioning, in accordance with the established design objectives. Since both mechanisms are intended to be operated together as a combined system, it is essential that the number of precision points defining the motion requirements is identical for both phases. Accordingly, the kinematic synthesis for the swing phase considers three precision points, necessitating the definition of three unknown parameters. As illustrated in Figure 3, these parameters are identified as ρ_F, ϕ_F, and r_5. Parameter r_4 is designated as an optimization variable, while the other three parameters are treated as unknowns to ensure that the combined mechanism achieves the desired motion seamlessly. This part is dedicated to make sure the stance movement is achieved by the proposed mechanism that is synthesized. During the swing phase, the mechanism continues its motion as designed, with the ED link initially aligned in the desired orientation.

To accommodate the combined mechanism's movement, the shared dyad r_3, previously established for the stance phase, can be integrated into the kinematic analysis. This integration ensures the continuity and alignment of the motion requirements for both phases.

The closed-loop equations for the x and y coordinates and angle relations are given in Equations (27) and (28):

$$\rho_F \mathrm{c}\phi_F + r_5 \mathrm{c}\theta_5 = r_3 \mathrm{c}\theta_3 + r_4 \mathrm{c}\theta_4 \tag{27}$$

$$\rho_F \mathrm{s}\phi_F + r_5 \mathrm{s}\theta_5 = r_3 \mathrm{s}\theta_3 + r_4 \mathrm{s}\theta_4 \tag{28}$$

As seen in Table 2, we tried to achieved the results with three precision points for three structural parameters.

Table 2. Swing phase design parameters classification.

Classification	Parameters
Construction Parameters	ρ_F, ϕ_F, r_5
Known Parameters	r_4
Known Variables	θ_3, θ_4
Unknown Variable	θ_5

The objective function is reached as a result of adding the squares of Equations (27) and (28), eliminating θ_5 as a result, and arranging them according to the known and unknown parameters and variables specified in Table 2 (Equation (29)).

$$\frac{r_4^2+\rho_F^2-r_5^2}{2}+(\rho_F c_F)[-r_3 c\theta_3 - r_4 c\theta_4]+(\rho_F s_F)[-r_3 s\theta_3 - r_4 s\theta_4]-\left[-r_3 r_4 c(\theta_3-\theta_4)-\frac{r_3^2}{2}\right]=0 \quad (29)$$

The representation of Equation (29) in polynomial form is presented in Equation (30):

$$P_0 f_0 + P_1 f_1 + P_2 f_2 - F = 0 \quad (30)$$

The polynomial constants and variable functions in Equation (30) are shown collectively in Equation (31):

$$\begin{gathered} P_0 = \tfrac{r_4^2+\rho_F^2-r_5^2}{2}, \quad f_0 = 1 \\ P_1 = \rho_F c\text{ø}_F, \quad f_1 = -r_3 c\theta_3 - r_4 c\theta_4 \\ P_2 = \rho_F s\text{ø}_F, \quad f_2 = -r_3 s\theta_3 - r_4 s\theta_4 \\ F = -r_3 r_4 c(\theta_3-\theta_4)-\tfrac{r_3^2}{2} \end{gathered} \quad (31)$$

In order to solve three construction parameters r_4, r_5, and ρ_F that are included in P_0, P_1, and P_2, three precision points are needed to evaluate the related variable functions of Equation (30) to form three equation sets (Equation (32)):

$$\begin{bmatrix} f_0^1 & f_1^1 & f_2^1 \\ f_0^2 & f_1^2 & f_2^2 \\ f_0^3 & f_1^3 & f_2^3 \end{bmatrix} \begin{bmatrix} P_0 \\ P_1 \\ P_2 \end{bmatrix} = \begin{bmatrix} F_1 \\ F_2 \\ F_3 \end{bmatrix} \quad (32)$$

Solving Equation (32) along with Equation (31), unknown construction parameters can be found (Equation (33)):

$$\begin{gathered} \text{ø}_F = \text{atan2}(P_2, P_1) \\ \rho_F = \tfrac{P_1}{\cos \text{ø}_F} \,//\, \rho_F = \tfrac{P_2}{\sin \text{ø}_F} \\ r_5 = \sqrt{r_4^2+\rho_F^2-2P_0} \end{gathered} \quad (33)$$

When the common three precision points are selected for both phase systems, the combined mechanism functions as a single-DoF system, achieving the stance phase movement with the required orientation for a seamless transition to the swing phase.

On the other hand, upon entering the swing phase, it becomes necessary for the ICR to be aligned with the centroid of the biological knee. In order to accomplish this, the second loop of the combined system should become a single four-bar mechanism without having any constraints from the first loop to maintain this desired motion. This configuration is only possible if the length of dyad r_1 is allowed to be changed with a prismatic joint throughout the swing phase, while the length of the dyad r_3 becomes constant. Thus, once the swing phase begins, the r_3 parameter must continue its movement as a fixed length to ensure that the system functions as a purely anti-parallel four-bar mechanism. The method for implementing this constraint is addressed in the following section on conceptual design.

4. Conceptual Design and Simulation Results

As mentioned in the previous sections, the final design integrates kinematic synthesis to construct a two-DoF five-bar mechanism for a stable ICR and coupler orientation during stance, which is then reduced to one DoF by a shared dyad that locks r_3 during the swing phase while maintaining system mobility. This is achieved by freeing r_1 to allow natural

ICR tracking in the swing phase mode. Considering the coarse representation as illustrated in Figure 4a, during the stance phase of the gait, a higher-force closed kinematic pair with a point contact will be formed at point C′, similar to a cam-follower system. When the motion transitions from stance to swing, point C′ will lose its point of contact, becoming a free point in the planar subspace, while, at the same instance, a higher-force closed kinematic pair with a point contact will be formed at point D′. This way, the overall DoFs of the mechanism will be retained as one. Due to the nature of the force closed kinematic pairs that are prone to disassembly during the absence of required forces, in the proposed mechanism shown in Figure 4b, instead of utilizing a cam surface, a slot was selected to be used with the same profile. Furthermore, as additional special cases, in order to simplify the synthesis complexity, circular profiles with centers located at A and B points, respectively, were formed. With the help of this configuration, prismatic joint motion constraints were achieved; that is, during the stance phase when C′ is in a slot, the prismatic joint connected to the CC′ dyad will be locked, while the prismatic joint connected to the DD′ dyad will be capable of linear motion. During the swing phase, the condition will be reversed, as, when D′ is in a slot, the prismatic joint connected to the DD′ dyad will be locked, while the prismatic joint connected to the CC′ dyad will be capable of linear motion.

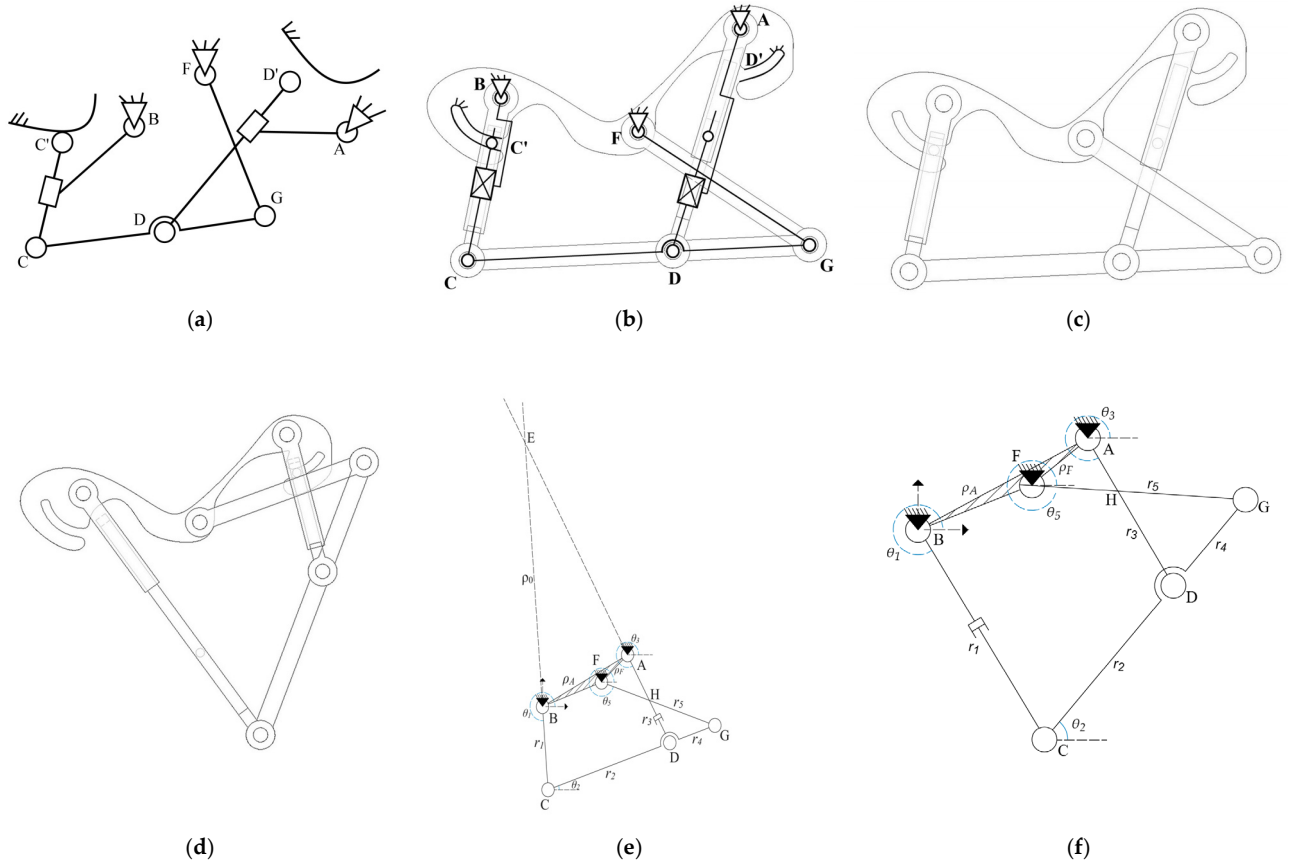


Figure 4. (**a**) Proposed single-DoF mechanism coarse representation; (**b**) proposed kinematic solution for single-DoF combined mechanism; (**c**) kinematic structure during stance phase; (**d**) kinematic structure during swing phase; (**e**) stance phase kinematic structure [48]; and (**f**) swing phase kinematic structure.

The rigid body containing joint A, joint B, and joint F represents the fixed grounding. The transition between the stance and swing phases are illustrated in Figure 4c and 4d, respectively. Simplified kinematic representations for both the stance and swing phases can

be seen in Figure 4e and 4f, respectively; as such, r_1 is turned into a prismatic joint from a regular link, while r_3 is transformed into a fixed-length link from a prismatic joint.

This engineering approach necessitates two distinct kinematic analyses to ensure a complete motion analysis by keeping the overall mobility as one but changing its structure. These analyses enable the simulation of the system's movement, facilitating the extraction of motion and orientation errors and the evaluation of the flexion stability ratio. Ultimately, the optimization methods can be integrated to refine the design and enhance the system performance.

4.1. Kinematic Analysis for Overall Mechanism

Although the common rod angle (θ_3) serves as the input in the actual application, for simplifying the position analysis, the flexion angle (θ_2) is selected as the input angle, given that its limits are predefined. During the stance phase ($\theta_2 \leq \theta_{2n}$), the relationship between the input and output can be expressed using distinct functions ($\theta_3 = f(\theta_5)$; $r_3 = g(\theta_3, \theta_5)$) derived from the second closed kinematic loop, as formulated in Equations (27) and (28). Since the closed loops are interdependent, the position analysis within its kinematic structure is relatively straightforward. The values of θ_5, θ_1, θ_3, and r_3 are subsequently determined using Equation (34):

$$\begin{gathered} \theta_5 = 2atan\left(\frac{-B \pm \sqrt{B^2-4AC}}{2A}\right) \\ \theta_1 = atan2\begin{pmatrix} \rho_F \mathrm{s}\varnothing_F + \rho_A \mathrm{s}\varnothing_A + r_5 \mathrm{s}\theta_5 - (\mathrm{r}_2 + r_4)\mathrm{s}\theta_2, \\ \rho_F \mathrm{c}\varnothing_F + \rho_A \mathrm{c}\varnothing_A + r_5 \mathrm{c}\theta_5 - (\mathrm{r}_2 + r_4)\mathrm{c}\theta_2 \end{pmatrix} \\ \theta_3 = atan2\begin{pmatrix} \rho_F \mathrm{s}\varnothing_F + r_5 \mathrm{s}\theta_5 - r_4 \mathrm{s}\theta_2, \\ \rho_F \mathrm{c}\varnothing_F + r_5 \mathrm{c}\theta_5 - r_4 \mathrm{c}\theta_2 \end{pmatrix} \\ r_3 = \frac{\rho_F \mathrm{s}\varnothing_F + r_5 \mathrm{s}\theta_5 - r_4 \mathrm{s}\theta_2}{\sin\theta_3} \;//\; r_3 = \frac{\rho_F \mathrm{c}\varnothing_F + r_5 \mathrm{c}\theta_5 - r_4 \mathrm{c}\theta_2}{\cos\theta_3} \end{gathered} \tag{34}$$

where

$$A = \rho_F r_5 \mathrm{c}\varnothing_F + \rho_A r_5 \mathrm{c}\varnothing_A - r_5(\mathrm{r}_2 + r_4)\mathrm{c}\theta_2 + \rho_F(\mathrm{r}_2 + r_4)\mathrm{c}(\varnothing_F - \theta_2) + \rho_A(\mathrm{r}_2 + r_4)\mathrm{c}(\varnothing_A - \theta_2) - \rho_A\rho_F \mathrm{c}(\varnothing_A - \varnothing_F) - \frac{\left(r_1^2 - \rho_F^2 - \rho_A^2 - r_5^2 - (\mathrm{r}_2 + r_4)^2\right)}{2}$$

$$B = -2(\rho_F r_5 \mathrm{s}\varnothing_F + \rho_A r_5 \mathrm{s}\varnothing_A - r_5(\mathrm{r}_2 + r_4)\mathrm{s}\theta_2)$$

$$C = r_5(\mathrm{r}_2 + r_4)\mathrm{c}\theta_2 - \rho_F r_5 \mathrm{c}\varnothing_F - \rho_A r_5 \mathrm{c}\varnothing_A - \rho_F(\mathrm{r}_2 + r_4)\mathrm{c}(\varnothing_F - \theta_2) + \rho_A(\mathrm{r}_2 + r_4)\mathrm{c}(\varnothing_A - \theta_2) - \rho_A\rho_F \mathrm{c}(\varnothing_A - \varnothing_F) - \frac{\left(r_1^2 - \rho_F^2 - \rho_A^2 - r_5^2 - (\mathrm{r}_2 + r_4)^2\right)}{2}$$

For the swing phase ($\theta_2 > \theta_{2n}$), the input–output relationship can be expressed through alternative functions due to changes in the mechanism structure. As previously mentioned, the prismatic joint r_3 is locked at the termination of the stance phase, during which its kinematic pair type alters. Simultaneously, to maintain a single-DoF by changing the kinematic structure, joint C is released in the longitudinal direction, functioning as a lower kinematic pair. The position analysis for the closed loops in this configuration can be determined using Equation (35), in order to find values of θ_3, θ_5, r_1, and θ_1:

$$\begin{gathered}\theta_3 = 2atan\left(\frac{-B\pm\sqrt{B^2-4AC}}{2A}\right)\\ \theta_5 = atan2\begin{pmatrix}\mathrm{r}_3\mathrm{s}\theta_3 + r_4\mathrm{s}\theta_2 - \rho_F\mathrm{s}\varnothing_F,\\ \mathrm{r}_3\mathrm{c}\theta_3 + r_4\mathrm{c}\theta_2 - \rho_F\mathrm{c}\varnothing_F\end{pmatrix}\\ r_1 = \sqrt{\rho_A^2 + r_3^2 + r_2^2 + 2\rho_A r_3\mathrm{c}(\varnothing_A - \theta_3) - 2\rho_A r_2\mathrm{c}(\varnothing_A - \theta_2) - 2r_2 r_3\mathrm{c}(\theta_2 - \theta_3)}\\ \theta_1 = atan2\begin{pmatrix}\rho_A\mathrm{s}\varnothing_A + r_3\mathrm{s}\theta_3 - r_2\mathrm{s}\theta_2,\\ \rho_A\mathrm{c}\varnothing_A + r_3\mathrm{c}\theta_3 - r_2\mathrm{c}\theta_2\end{pmatrix}\end{gathered} \tag{35}$$

where

$$A = r_3 r_4\mathrm{c}\theta_2 - r_3\rho_F\mathrm{c}\varnothing_F + r_4\rho_F\mathrm{c}(\theta_2 - \varnothing_F) - \frac{\left(r_3^2+r_4^2+\rho_F^2-r_5^2\right)}{2}$$

$$B = -2(r_3 r_4\mathrm{s}\theta_2 - r_3\rho_F\mathrm{s}\varnothing_F)$$

$$C = -r_3 r_4\mathrm{c}\theta_2 + r_3\rho_F\mathrm{c}\varnothing_F + r_4\rho_F\mathrm{c}(\theta_2 - \varnothing_F) - \frac{\left(r_3^2+r_4^2+\rho_F^2-r_5^2\right)}{2}$$

The combined mechanism exhibits two distinct structural configurations, maintaining its mobility. This adaptability underscores the mechanism's ability to satisfy the diverse phase requirements through a dynamic structural reconfiguration. To validate and further explore its functionality, a numerical implementation is employed, enabling a detailed examination of the working principle.

Through a numerical analysis, critical parameters such as positional accuracy, orientation consistency, and the effectiveness of the phase transitions can be evaluated. Additionally, motion simulations are conducted to identify potential deviations or inefficiencies in the mechanism's behavior under varying conditions. These simulations provide a foundation for optimization, ensuring that the mechanism achieves the desired biomechanical reliability and operational robustness. The subsequent section details the numerical approach and simulation outcomes, highlighting the mechanism's performance and areas for refinement.

4.2. Numerical Approach and Simulation

Numerical implementation is a crucial step in validating the theoretical framework established through kinematic synthesis and analysis. By translating the derived equations into computational algorithms, the mechanism's behavior can be simulated under various conditions, allowing for a complete evaluation of its performance. In this study, MATLAB (ver. 2023b) was utilized to program kinematic equations, enabling the systematic analysis of both the stance and swing phase transitions. The results obtained from these numerical simulations provide valuable insights into the mechanism's motion characteristics, positional accuracy, and phase transition kinematics, forming the basis for further optimization and validation efforts. Additionally, using the same program, kinematic motions were visualized, establishing MATLAB (ver. 2023b) as a visual simulation tool for the mechanism. A model of an average-sized leg was combined to enhance aesthetic realism, allowing the visualization to consider potential sizing errors and improve the design's alignment with realistic sizes.

As outlined in the kinematic synthesis and analysis sections, certain variables must be optimized to achieve more efficient and functional solutions. To validate the proposed methodology, an example solution was derived based on the specified variables, precision points, and required parameters. These details are summarized in Table 3, providing a clear reference for the implementation and results of the approach.

Table 3. Design parameters for example application.

Parameter	Value
Offset of Point B from Origin	X: −10 mm; Y: 10 mm
Flexion Angle Offset	−10°
Precision Point 1	X_1; Y_1 (20.0 mm; 128.0 mm); $\theta_2 = 0°$
Precision Point 2	X_2; Y_2 (−16.6 mm; 123.9 mm); $\theta_2 = 5°$
Precision Point 3 (Transition Point)	X_3; Y_3 (−30.0 mm; 70.0 mm); $\theta_2 = 20°$
Knee Centroid Point at Transition	X_H; Y_H (28.3 mm; −20.9 mm)
r_4	10 mm

The procedural steps and outcomes of the MATLAB (ver. 2023b) script utilizing the design parameters outlined in Table 3 are depicted in Figure 5, providing a detailed visualization of the methodology. The x component of the origin point is aligned along with the axis extending from the hip to the ankle, while the y component corresponds to the location of the center of the lateral femoral condyle. These dimensions and axes are illustrated in Figure 5a, where precision points and the transition instance are plotted on an average-sized leg for visualization within the sagittal plane. In the kinematic synthesis process, point B, defined as the mechanism's origin, serves as a reference point in mathematical models but can be adaptably positioned on the knee for flexibility in generating diverse solutions. For clarity, the origin in this example application differs from the defined ground origin, indicated in Figure 5a marked with a ground symbol. Hip and ankle centers are indicated along the y-axis, while the lateral femoral condyle center shapes the x-axis. Although no strictly defined ICR trajectory exists, its characteristics depend on patient-specific factors such as activity level, residual limb dimensions, and lifestyle. The critical feature of the trajectory is that it must ensure natural stability during the stance phase. Figure 5a shows three precision points, indicated as red dots, derived from the trajectory of a commercial passive polycentric transfemoral prosthesis, validating the methodology only within a stance phase interval of 0° to 20° flexion. Additionally, one more red dot, point H in Table 3, is also indicated, which stands for the natural ICR point to be utilized in the swing phase mechanism at the transition instance, defining 20° flexion for the simulation of numerical validation. It is expected to orient the shared member through the virtual line from the third precision point of the stability ICR trajectory and the natural ICR point defined for the swing phase beginning. The orientation line is indicated as dashed black line in Figure 5a.

After the utilization of the kinematic synthesis methodology with specified demonstration parameters, the results are obtained and presented. In Figure 5b, three precision points, their corresponding poses for the stance phase mechanism (a five-bar linkage with a variable r_3 link), and the transition pose are shown. Here, the alignment of the third precision point with the transition point is emphasized as a critical requirement. Furthermore, an offset angle is introduced at the pylon tube–foot connection to adjust the required knee flexion. In this example, the offset angle is set to a non-zero value for better demonstration. The coupler link r_2, represented in blue, begins with the mentioned offset angle as defined in Table 3 and ends with the 20° total flexion angle change.

The trajectory of motion is illustrated in Figure 5c with the corresponding x and y components represented as black dots on the sagittal plane, where the r_3 link length varies linearly in moderate steps. At the transition point, the shared member's orientation aligns as required, pointing towards the predefined knee centroid for the swing phase. Depending on the results given in the stance phase, the kinematic synthesis procedure for the swing phase mechanism is utilized, in which the r_4 link member is selected as an optimization parameter given in Table 3 to shape the swing phase mechanism, ensuring alignment with the desired kinematic behavior. The extracted results of the final combined mechanism

are kinematically visualized on the sagittal plane with placing on an average-sized leg in Figure 5d, which makes the whole system single-DoF.

The simulation results in Figure 5e demonstrate the stance phase ICR stability (black dots) and the swing phase ICR alignment (red dots) through the full range of motion from 0° to 120° flexion. At the stance phase's end, corresponding 120° flexion, r_1 extends to preserve mobility, while r_3 locks along the prismatic direction.

Figure 5f evaluates the full flexion position, confirming the design's dimensional feasibility for manufacturing and integration with human anatomy. The results validate the singularity-free motion across the range, demonstrating the theoretical applicability.

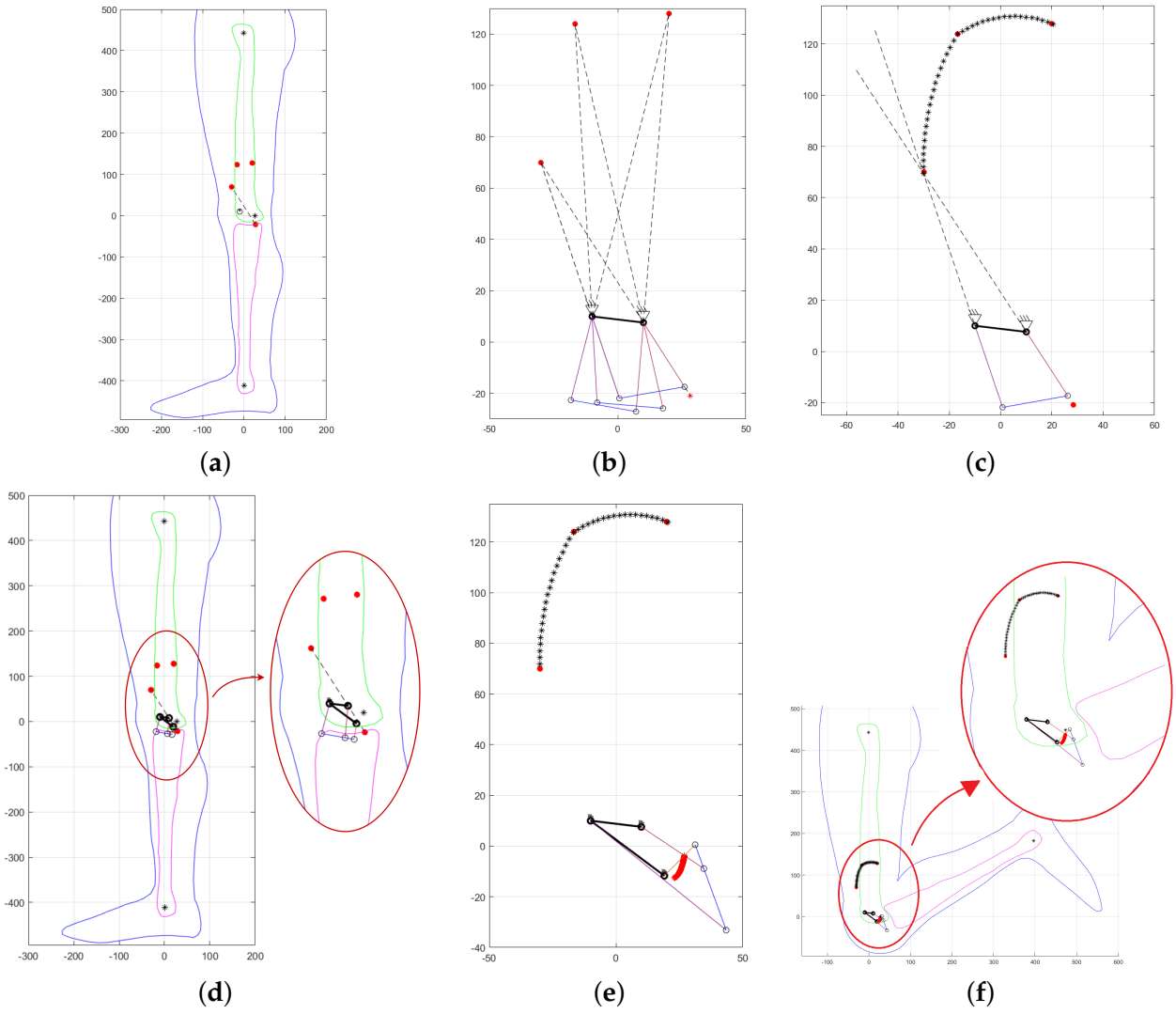


Figure 5. The procedural approach and comprehensive visualization of an example application: (**a**) Plane definition, precision points and transition moment on an average-sized leg to visualize their distribution on the sagittal plane; (**b**) Three precision points, their corresponding poses for the stance phase mechanism and the transition pose after the completion of the kinematic synthesis procedure; (**c**) The trajectory of ICR motion with corresponding x and y components represented as black dots on the sagittal plane, where the r_3 link length varies linearly in moderate steps; (**d**) Mechanism's overall dimensions relative to an average-sized leg in full extension; (**e**) Constructed and simulated combined mechanism by integrating the stance phase mechanism with the swing phase parameter r_4; (**f**) Mechanism's overall dimensions relative to an average-sized leg in 120° flexion.

The applicability of the proposed conceptual design in terms of kinematics has been demonstrated. The mathematical model for kinematic synthesis was integrated with a numerical example to visualize the results on an average-sized human leg, highlighting that the kinematic synthesis methodology imposes no inherent dimensional constraints or boundaries. Visualization was achieved using MATLAB (ver. 2023b) based simulations. This study underscores the importance of incorporating multiple optimization parameters and refining trajectory design to achieve full motion capabilities. To facilitate this process, the authors developed a MATLAB-based graphical user interface, enabling designers to define parameters, optimize mechanisms and compare outcomes across different designs [55]. Comprehensive optimization and dynamic analyses were identified as essential next steps and are left to future work. These efforts will deepen the analysis, integrate the graphical user interface and provide a robust foundation for real-world experimental validation.

5. Discussions

The current study introduces a novel approach to the kinematic synthesis and design of a modular polycentric knee mechanism for transfemoral prostheses. The discussion focuses on evaluating the outcomes in the context of the stated objectives, exploring design trade-offs and addressing limitation, while also suggesting potential directions for future research.

One of the primary achievements of this study is the development of a combined mechanism that seamlessly integrates the distinct kinematic requirements for the stance and swing phases into a single-DoF structure. This innovative design enables the mechanism to be able to take to different configurations during the transition between the stance and swing phases, as explained in Section 3, effectively avoiding singularity points during full knee flexion. The modular nature of the mechanism further ensures the adaptability to various user characteristics, such as anatomical differences and activity levels, while maintaining robustness and precision across gait cycles.

The proposed approach demonstrates significant potential in improving both stability and motion biomimicry. The polycentric stance mechanism, which leverages a strategically positioned ICR, provides enhanced weight-bearing stability and secure positioning during the stance phase. Meanwhile, the swing mechanism's biomimetic trajectory aligns with the requirements of natural knee movement, ensuring smoother transitions between gait phases.

Compared to existing single-DoF knee mechanisms, the proposed design uniquely addresses the challenge of singularity avoidance, which is often overlooked in the development of polycentric systems. While cam-based designs focus on precise ICR control and linkage-based approaches prioritize structural simplicity, this study combines the strength of both methodologies. By integrating analytical kinematic synthesis, the mechanism achieves a balance between functional complexity and manufacturability. Additionally, the modular structure sets this design apart from the conventional fixed-geometry mechanism. Unlike standard prostheses, which are typically tuned for generic users, the proposed mechanism can be customized for individual needs without compromising the overall performance.

Despite the promising results, several limitations and challenges remain for further investigation. The reliance on a prismatic joint introduces potential concerns regarding wear and maintenance, particularly under high-load conditions. Furthermore, while the MATLAB-based numerical analyses and simulation provide a detailed understanding of the mechanism's behavior, real-world validations, including fatigue tests and user trials, are essential in order to fully assess its durability and functionality. The analysis in the

future must consist of following additional metrics such as durability, adaptability, and user comfort.

One more notable limitation is the absence of a dynamic analysis in this study. While the kinematic analysis and simulations provide a strong theoretical groundwork, they do not fully account for inertial effects, impact forces, or other dynamic factors that occur during real-world usage. Incorporating dynamic modeling would enable a more comprehensive understanding of the mechanism's behavior, particularly during rapid transitions between the stance and swing phases.

Another critical consideration is the impact of phase transitions on user experience and overall gait smoothness. Although the proposed design ensures seamless phase transitions in theory, the practical implications of these transitions, such as potential discomfort, delays, or instability during use, remain unexplored. Experimental studies involving users could show how these transitions affect functionality and comfort, providing valuable insights for refining the design. It should be noted for the readers that a common issue related with reconfigurable mechanisms [56–58] such as the proposed mechanism in the manuscript is the possibility to encounter large forces. Thus, an optimization procedure should be followed for the final design that is synthesized with patient-specific data. In order to achieve an efficient transition to the final mechanism, mechanical slots should be designed in a way that they will cover a portion of the motion as a dependent geometry; that is, both of the pins should be in guided slots at the same time during prescribed parts of the motion. This is possible via executing a kinematic analysis on the final structure and choosing pin locations on related links that will generate paths with less pointed geometries. The later remaining (if they exist) pointed ends of the slot curves can be smoothened to allow a controlled intentional error in the final path of the mechanism. For the stance case, as the main target lies in achieving the ICR at a distant location, an injected error to smoothen the transition at prescribed locations will not affect the overall design constraints. On the other hand, for the swing phase, this generated error should also be taken as an additional optimization parameter.

While the addition of an actuator is planned for future iterations to enable active actuation, it is important to emphasize that the mechanism is designed to function without an actuator as well due to the fact that actuation is not strongly required during ground-level walking. Ensuring effective performance is also essential in a non-powered (or low-powered to exceed the effects on elastic components) actuator configuration. This dual functionality raises additional questions about how the phase transitions and overall performance are influenced by the presence or absence of an actuator, suggesting an area for further research.

By addressing these limitations, future iterations of the design can enhance its robustness, adaptability, and user satisfaction, ensuring that the mechanism meets diverse needs and performs reliably in various real-world scenarios.

6. Conclusions

This study presents a novel methodology for the design of a transfemoral prosthetic knee mechanism, aiming to address the dual challenges of stability and biomimetic motion through an analytically derived polycentric design. By integrating separate structural models for the stance and swing phases into a combined mechanism with a single-DoF, the proposed system offers an innovative solution that avoids singularities during knee flexion, which is a key limitation in conventional active designs. This approach not only ensures stability during the stance phase through robust ICR trajectory control but also facilitates natural biomimetic motion in the swing phase by incorporating insights from orthotic applications and polycentric knee mechanisms.

The modular framework developed in this study enables the personalized adaptation of the mechanism based on individual user characteristic, such as weight, activity level, and anatomical differences. Furthermore, the integration of analytical kinematic synthesis methods allows for user-specific adjustments to the flexion angle and overall functionality, ensuring that the prosthesis can meet diverse gait phase requirements with enhanced functionality, offering a versatile design procedure allowing for a more efficient approach for patient-specific designs and avoiding the singularity point during full flexion.

The design's compatibility with motorized actuation further places it as a possible candidate for the active polycentric knee mechanism, enabling adaptive control for improved performance across dynamic conditions. This feature not only advances the biomechanical utility of the mechanism but also lays the groundwork for future research and development in the motorized transfemoral prosthetic system.

Overall, the proposed methodology provides a scientifically robust base for the development of the possible future use of transfemoral prostheses. By harmonizing the stability, adaptability, and biomimetic motion, this study offers a promising pathway toward improving the quality of life for lower limb amputees, enhancing both prosthetic functionality and user comfort.

Author Contributions: Conceptualization, M.K. and E.G.; methodology, M.K. and E.G.; software, M.K.; validation, M.K. and E.G.; formal analysis, M.K. and E.G.; investigation, M.K. and E.G.; resources, M.K. and E.G.; data curation, M.K. and E.G.; writing—original draft preparation, M.K. and E.G.; writing—review and editing, M.K. and E.G.; visualization, M.K. and E.G.; supervision, E.G.; project administration, E.G.; funding acquisition, E.G. All authors have read and agreed to the published version of the manuscript.

Funding: This research has been financially supported by İzmir Kâtip Çelebi University (project number: 2023-TDR-MÜMF-0019).

Data Availability Statement: The data presented in this study are available upon request from the corresponding author.

Acknowledgments: During the preparation of this manuscript, the authors used ChatGPT [https://chatgpt.com/ (accessed on 1 December 2024)] for the purposes of enhancing the English language in some parts of the paper for clarity in presentation. It should be strictly noted that the written text by the authors was only modified in terms of grammar via generative AI in the related parts of the paper.

Conflicts of Interest: The authors declare no conflicts of interest.

References

1. Soriano, J.F.; Rodríguez, J.E.; Valencia, L.A. Performance comparison and design of an optimal polycentric knee mechanism. *J. Braz. Soc. Mech. Sci. Eng.* **2020**, *42*, 221. [CrossRef]
2. Yuan, B.; Hu, D.; Gu, S.; Xiao, S.; Song, F. The global burden of traumatic amputation in 204 countries and territories. *Front. Public Health* **2023**, *11*, 1258853. [CrossRef] [PubMed]
3. Kim, Y.C.; Park, C.I.; Kim, D.Y.; Kim, T.S.; Shin, J.C. Statistical analysis of amputations and trends in Korea. *Prosthet. Orthot. Int.* **1996**, *20*, 88–95. [CrossRef] [PubMed]
4. Chien, M.C.H.; Erdemir, A.; van den Bogert, A.J.; Smith, W.A. Development of dynamic models of the Mauch prosthetic knee for prospective gait simulation. *J. Biomech.* **2014**, *47*, 3178–3184. [CrossRef]
5. Cumming, J.; Barr, S.; Howe, T.E. Prosthetic rehabilitation for older dysvascular people following a unilateral transfemoral amputation. *Cochrane Database Syst. Rev.* **2006**, *4*. [CrossRef]
6. Pasquina, C.P.F.; Carvalho, A.J.; Sheehan, T.P. Ethics in rehabilitation: Access to prosthetics and quality care following amputation. *AMA J. Ethics* **2015**, *17*, 535–546.
7. McDonald, C.L.; Westcott-McCoy, S.; Weaver, M.R.; Haagsma, J.; Kartin, D. Global prevalence of traumatic non-fatal limb amputation. *Prosthet. Orthot. Int.* **2021**, *45*, 105–114. [CrossRef]

8. Awad, M.I.; Abouhossein, A.; Dehghani-Sanij, A.A.; Richardson, R.; Moser, D.; Zahedi, S.; Bradley, D. Towards a smart semi-active prosthetic leg: Preliminary assessment and testing. *IFAC-PapersOnLine* **2016**, *49*, 170–176. [CrossRef]
9. Lara-Barrios, C.M.; Blanco-Ortega, A.; Guzmán-Valdivia, C.H.; Bustamante Valles, K.D. Literature review and current trends on transfemoral powered prosthetics. *Adv. Robot.* **2018**, *32*, 51–62. [CrossRef]
10. Lura, D.J.; Wernke, M.M.; Carey, S.L.; Kahle, J.T.; Miro, R.M.; Highsmith, M.J. Differences in knee flexion between the Genium and C-Leg microprocessor knees while walking on level ground and ramps. *Clin. Biomech.* **2015**, *30*, 175–181. [CrossRef]
11. Poliakov, A.; Ryzhkov, A.; Kolesova, M.; Shtanko, P.; Sopin, P.; Bugayov, P. Novel Design of an Active Transfemoral Prosthesis with Intellectual-Synergetic Control System. In Proceedings of the 2020 International Conference on Electrical, Communication, and Computer Engineering (ICECCE), Istanbul, Turkey, 12–13 June 2020; IEEE: Piscataway, NJ, USA, 2020; pp. 1–6.
12. Anand, T.S.; Sujatha, S. A method for performance comparison of polycentric knees and its application to the design of a knee for developing countries. *Prosthet. Orthot. Int.* **2017**, *41*, 402–411. [CrossRef] [PubMed]
13. Radcliffe, C.W.; Deg, M.E. Biomechanics of Knee Stability Control with Four-bar Prosthetic Knees. In Proceedings of the ISPO Australia Annual Meeting, Melbourne, Australia, 27–29 November 2003; Volume 11, pp. 1–25.
14. Ruiz-Díaz, F.D.; Altamirano-Altamirano, A.; Valentino-Orozco, G.A. External Knee Prosthesis with Four Bar Linkage Mechanism. In Proceedings of the 2016 13th International Conference on Electrical Engineering, Computing Science and Automatic Control (CCE), Mexico City, Mexico, 26–30 September 2016; IEEE: Piscataway, NJ, USA, 2016; pp. 1–6.
15. Greene, M.P. Four bar linkage knee analysis. *Orthot. Prosthet.* **1983**, *37*, 15–24.
16. Bapat, G.M.; Sujatha, S. A method for optimal synthesis of a biomimetic four-bar linkage knee for a knee-ankle-foot orthosis. *J. Biomim. Biomater. Biomed. Eng.* **2017**, *32*, 20–28. [CrossRef]
17. Poliakov, A.; Pakhaliuk, V.; Lozinskiy, N.; Kolesova, M.; Bugayov, P.; Shtanko, P. Biosimilar artificial knee for transfemoral prostheses and exoskeletons. *Facta Univ. Ser. Mech. Eng.* **2016**, *14*, 321–328. [CrossRef]
18. Radcliffe, C.W. Four-bar linkage prosthetic knee mechanisms: Kinematics, alignment and prescription criteria. *Prosthet. Orthot. Int.* **1994**, *18*, 159–173. [CrossRef]
19. Gard, S.A.; Childress, D.S.; Uellendahl, J.E. The influence of four-bar linkage knees on prosthetic swing-phase floor clearance. *JPO J. Prosthet. Orthot.* **1996**, *8*, 34–40. [CrossRef]
20. Sensinger, J.W.; Intawachirarat, N.; Gard, S.A. Contribution of prosthetic knee and ankle mechanisms to swing-phase foot clearance. *IEEE Trans. Neural Syst. Rehabil. Eng.* **2012**, *21*, 74–80. [CrossRef]
21. Bernal-Torres, M.G.; Medellín-Castillo, H.I.; Arellano-González, J.C. Development of an Active Biomimetic-Controlled Transfemoral Knee Prosthesis. In Proceedings of the ASME International Mechanical Engineering Congress and Exposition, Phoenix, AZ, USA, 11–17 November 2016; American Society of Mechanical Engineers: New York, NY, USA, 2016; Volume 50534, p. V003T04A057.
22. Morales-Cruz, C.; Portilla-Flores, E.A.; Suárez-Santillán, R.A.; Hernández-Oliva, N.; Calva-Yáñez, M.B. Synthesis of a Non-Grashof Six-Bar Polycentric Knee Prostheses Using an Evolutionary Optimization Algorithm. In Proceedings of the EngOpt 2018 Proceedings of the 6th International Conference on Engineering Optimization, Lisboa, Portugal, 17–19 September 2018; Springer International Publishing: Berlin/Heidelberg, Germany, 2018; pp. 1121–1132.
23. Sancisi, N.; Caminati, R.; Parenti-Castelli, V. Optimal Four-Bar Linkage for the Stability and the Motion of the Human Knee Prostheses. In Proceedings of the Atti del XIX CONGRESSO dell'Associazione Italiana di Meccanica Teorica e Applicata, Ancona, Italy, 14–17 September 2009; pp. 1–10.
24. Marisami, P.; Venkatachalam, R. Towards optimal toe-clearance in synthesizing polycentric prosthetic knee mechanism. *Comput. Methods Biomech. Biomed. Eng.* **2022**, *25*, 656–667. [CrossRef]
25. Wang, X.; Zhang, Y.; Liang, W.; Chen, W.; Xiu, H.; Ren, L.; Wei, G.; Ren, L. Design, control, and validation of a polycentric hybrid knee prostehsis. *IEEE Trans. Ind. Electron.* **2022**, *70*, 9203–9214. [CrossRef]
26. Chauhan, S.S.; Khare, A.K. Analysis of four-bar linkages suitable for above-knee prosthesis. *Evergreen* **2022**, *9*, 737–744. [CrossRef]
27. Phoengsongkhro, S.; Tangpornprasert, P.; Yotnuengnit, P.; Samala, M.; Virulsri, C. Development of four-bar polycentric knee joint with stance-phase knee flexion. *Sci. Rep.* **2023**, *13*, 22809. [CrossRef] [PubMed]
28. Mohamed, N.; Alateyah, A.I.; El-Garaihy, W.H. Defect free optimization of a polycentric prosthetic knee design using imperialist competition-inspired optimization method. *J. Eng. Res.* **2023**, *11*. [CrossRef]
29. Ayğahoğlu, M.E.; Gümüş, M.S.; Çakan, A.; Kalyoncu, M. Dimension optimization of polycentric knee mechanism using the bees algorithm and genetic algorithm. *J. Mater. Mechatron. A* **2023**, *4*, 318–332. [CrossRef]
30. Zhang, Y.; Wang, E.; Wang, M.; Liu, S.; Ge, W. Design and experimental research of knee joint prosthesis based on gait acquisition technology. *Biomimetics* **2021**, *6*, 28. [CrossRef]
31. Ghaemi, N.; Dardel, M.; Ghasemi, M.H.; Zohoor, H. Optimization of six bar knee linkage for stability of knee prosthesis. *Majlesi J. Mechatron. Syst.* **2012**, *1*. Available online: https://ms.majlesi.info/index.php/ms/article/view/44 (accessed on 1 December 2024).

32. Eqra, N.; Abiri, A.H.; Vatankhah, R. Optimal synthesis of a four-bar linkage for path generation using adaptive PSO. *J. Braz. Soc. Mech. Sci. Eng.* **2018**, *40*, 469. [CrossRef]
33. Hobson, D.A.; Torfason, L.E. Optimization of four-bar knee mechanisms—A computerized approach. *J. Biomech.* **1974**, *7*, 371–376. [CrossRef]
34. Munoz-Cesar, J.J.; Hernández-Gómez, L.H.; López-Suárez, O.I.; Urriolagoitia-Sosa, G.; Beltrán-Fernández, J.A.; Urriolagoitia-Calderón, G.; Pava-Chipol, N.D.; Quintero-Gómez, I.J. Optimization of the design of a four bar mechanism for a lower limb prosthesis using the taboo search algorithm. In *Advances in Bio-Mechanical Systems and Materials*; Springer: Cham, Switzerland, 2013; pp. 107–125.
35. Radcliffe, C.W. Above-knee prosthetics. *Prosthet. Orthot. Int.* **1997**, *1*, 146–160. [CrossRef]
36. Imran, A.; Beigzadeh, B.; Haghjoo, M.R. A new passive transfemoral prosthesis mechanism based on 3R36 knee and ESAR foot providing walking and squatting. *Theor. Appl. Mech. Lett.* **2023**, *13*, 100476. [CrossRef]
37. Van Hal, E.S.; Hijmans, J.M.; Postema, K.; Otten, E. A passive polycentric mechanism to improve active mediolateral balance in prosthetic walking. *IEEE Trans. Neural Syst. Rehabil. Eng.* **2023**, *32*, 63–71. [CrossRef]
38. Windrich, M.; Grimmer, M.; Christ, O.; Rinderknecht, S.; Beckerle, P. Active lower limb prosthetics: A systematic review of design issues and solutions. *Biomed. Eng. Online* **2016**, *15*, 5–19. [CrossRef] [PubMed]
39. Geng, Y.; Xu, X.; Chen, L.; Yang, P. Design and Analysis of Active Transfemoral Prosthesis. In Proceedings of the IECON 2010-36th Annual Conference on IEEE Industrial Electronics Society, Glendale, AZ, USA, 7–10 November 2010; IEEE: Piscataway, NJ, USA, 2010; pp. 1495–1499.
40. Pfeifer, S.; Riener, R.; Vallery, H. An Actuated Transfemoral Prosthesis with Optimized Polycentric Knee Joint. In Proceedings of the 2012 4th IEEE Ras & EMBS International Conference on Biomedical Robotics and Biomechatronics (BioRob), Rome, Italy, 24–27 June 2012; IEEE: Piscataway, NJ, USA, 2012; pp. 1807–1812.
41. Wang, K.; Williams, H.; Qian, Z.; Wei, G.; Xiu, H.; Chen, W.; Lu, X.; Jin, J.; Ren, L.; Liang, W.; et al. Design and evaluation of a smooth-locking-based customizable prosthetic knee joint. *J. Mech. Robot.* **2024**, *16*, 041008. [CrossRef]
42. Hsu, Y.; Hung, Y.; Yin, J. Design of a novel total knee prosthesis using TRIZ. *J. Med. Biol. Eng.* **2006**, *26*, 177.
43. Hamill, J.; Knutzen, K.M. *Biomechanical Basis of Human Movement*; Lippincott Williams & Wilkins: Philadelphia, PA, USA, 2006.
44. Nordin, M.; Frankel, V.H. *Basic Biomechanics of the Muscoskeletal System*, 3rd ed.; Lippincott Williams & Wilkins: Philadelphia, PA, USA, 2001.
45. Walker, P.S.; Kurosawa, H.; Rovick, J.S.; Zimmerman, R.A. External knee joint design based on normal motion. *J. Rehabil. Res. Dev.* **1985**, *22*, 9–22. [CrossRef]
46. Olinski, M.; Gronowicz, A.; Ceccarelli, M. Development and characterization of a controllable adjustable knee joint mechanism. *Mech. Mach. Theory* **2021**, *155*, 104101. [CrossRef]
47. Bertomeu, J.M.B.; Lois, J.M.B.; Guillem, R.B.; Del Pozo, Á.P.; Lacuesta, J.; Mollá, C.G.; Luna, P.V.; Pastor, J.P. Development of a hinge compatible with the kinematics of the knee joint. *Prosthet. Orthot. Int.* **2007**, *31*, 371–383. [CrossRef]
48. Koçak, M.; Gezgin, E. Utilization of Kinematic Synthesis Methodology on a Novel Polycentric Mechanism for Transfemoral Knee Prosthesis. In Proceedings of the IFToMM Symposium on Mechanism Design for Robotics, Timişoara, Romania, 27–29 June 2024; Springer Nature: Cham, Switzerland, 2024; pp. 237–250.
49. Hartenberg, R.; Danavit, J. *Kinematic Synthesis of Linkages*; McGraw-Hill: New York, NY, USA, 1964.
50. Sandor, G.N.; Erdman, A.G. *Advanced Mechanism Design v.2: Analysis and Synthesis*; Prentice-Hall: Hoboken, NJ, USA, 1984.
51. Gezgin, E.; Yazıcı, M.V. Integration of the function generation synthesis into the design of a multi-leaf collimator. *J. Braz. Soc. Mech. Sci. Eng.* **2020**, *42*, 380. [CrossRef]
52. Koçak, M.; Yazıcı, M.V.; Akdal, E.; Can, F.C.; Gezgin, E. Utilization of function generation synthesis on biomimetics: A case study on moray eel double jaw design. *Biomimetics* **2022**, *7*, 145. [CrossRef]
53. Gezgin, E.; Chang, P.H.; Akhan, A.F. Synthesis of a Watt II six-bar linkage in the design of a hand rehabilitation robot. *Mech. Mach. Theory* **2016**, *104*, 177–189. [CrossRef]
54. Söylemez, E.; Kiper, G. Four-bar function generation using Excel solver. In Proceedings of the IFToMM World Congress on Mechanism and Machine Science, Tokyo, Japan, 5–10 November 2023; Springer Nature: Cham, Switzerland, 2023; pp. 208–218.
55. Koçak, M.; Gezgin, E. Development of a Graphical User Interface for Personalized Transfemoral Prosthesis Design. In Proceedings of the 1st IFToMM Young Faculty Group Symposium on Emerging Fields in Mechanism and Machine Science 2024, Online, 19–21 November 2024. [CrossRef]
56. Yin, H.; Yu, W.; Lyu, S.; Ding, X. Mobility, Singularity and Configuration Analysis of a Bennett-Based Reconfigurable 8R Linkage. In Proceedings of the 2024 6th International Conference on Reconfigurable Mechanisms and Robots (ReMAR), Chicago, IL, USA, 23–26 June 2024; IEEE: Piscataway, NJ, USA, 2024; pp. 473–478.

57. Wang, T.; Lin, Y.H.; Dai, J.S. Mathematical Modelling of a Four-Fingered Metamorphic Anthropomorphic Hand on Precision Grasp. In Proceedings of the 2024 6th International Conference on Reconfigurable Mechanisms and Robots (ReMAR), Chicago, IL, USA, 23–26 June 2024; IEEE: Piscataway, NJ, USA, 2024; pp. 619–624.
58. Wei, J.; Ni, H.; Zhang, J. Conformational Design and Kinematic Analysis of a Reconfigurable Ankle Rehabilitation Robot. In Proceedings of the 2024 6th International Conference on Reconfigurable Mechanisms and Robots (ReMAR), Chicago, IL, USA, 23–26 June 2024; IEEE: Piscataway, NJ, USA, 2024; pp. 479–486.

Disclaimer/Publisher's Note: The statements, opinions and data contained in all publications are solely those of the individual author(s) and contributor(s) and not of MDPI and/or the editor(s). MDPI and/or the editor(s) disclaim responsibility for any injury to people or property resulting from any ideas, methods, instructions or products referred to in the content.